

Symmetries in high-temperature lattice QCD with (u, d, s, c, b) optimal domain-wall quarks

Ting-Wai Chiu^{1,2,3,4,*}

¹*Department of Physics, National Taiwan Normal University,
Taipei, Taiwan 11677, Republic of China*

²*Institute of Physics, Academia Sinica, Taipei, Taiwan 11529, Republic of China*

³*Physics Division, National Center for Theoretical Sciences,
Taipei, Taiwan 10617, Republic of China*

⁴*Center for Theoretical Physics, Department of Physics, National Taiwan University,
Taipei, Taiwan 10617, Republic of China*

arXiv:2411.16705v1 [hep-lat] 18 Nov 2024

Abstract

The spatial z -correlators of meson operators in $N_f = 2 + 1 + 1 + 1$ lattice QCD with optimal domain-wall quarks are studied for eight temperatures in the range of 325-3250 MeV. The meson operators include a complete set of Dirac bilinears (scalar, pseudoscalar, vector, axial vector, tensor vector, and axial-tensor vector), and each for ten flavor combinations ($\bar{u}d, \bar{u}s, \bar{s}s, \bar{u}c, \bar{s}c, \bar{u}b, \bar{s}b, \bar{c}c, \bar{c}b, \bar{b}b$). We first observe the hierarchical restoration of chiral symmetry in QCD with (u, d, s, c, b) quarks, from $SU(2)_L \times SU(2)_R \times U(1)_A$ to $SU(3)_L \times SU(3)_R \times U(1)_A$, then to $SU(4)_L \times SU(4)_R \times U(1)_A$, and finally to $SU(5)_L \times SU(5)_R \times U(1)_A$, as the temperature is increased successively. Moreover, we study the emergence of the $SU(2)_{CS}$ chiral-spin symmetry, and compare the temperature windows for light and heavy vector mesons, and find that the temperature windows are dominated by the vector mesons of $\bar{u}b$ and $\bar{s}b$.

I. Introduction

To find out the symmetries in high temperature QCD is the first step in determining the properties and dynamics of matter under extreme conditions, which are crucial for understanding the mechanisms governing matter creation in the early universe and elucidating the outcomes of relativistic heavy ion collision experiments such as those at LHC and RHIC, as well as those of electron ion collision experiments at the planned electron-ion colliders. Lattice QCD provides the nonperturbative framework to find out the symmetries in high temperature QCD from the first principles. Since 1987 [1, 2], there have been many lattice studies using the screening masses of meson z -correlators to investigate the effective restoration of $U(1)_A$ and $SU(2)_L \times SU(2)_R$ chiral symmetries of u and d quarks in high temperature QCD, see, e.g., Ref. [3] and references therein. However, there were no discussions/studies in the literature about the hierarchical restoration of chiral symmetry in high temperature QCD, except for Refs. [4, 5].

Consider $N_f = 2 + 1 + 1 + 1$ QCD with nonzero quark masses, it does not possess the $SU(N)_L \times SU(N)_R \times U(1)_A$ chiral symmetry for any integer N from 2 to 5, due to the explicit symmetry breakings of the quark masses. However, as T is increased successively, each quark

* twchiu@phys.ntu.edu.tw

acquires thermal energy of the order of πT , and eventually its rest mass energy becomes negligible when $\pi T \gg m_q$. Also, since the quark masses range from a few MeV to a few GeV, it follows that as the temperature is increased successively, the chiral symmetry is restored hierarchically from $SU(2)_L \times SU(2)_R \times U(1)_A$ of (u, d) quarks to $SU(3)_L \times SU(3)_R \times U(1)_A$ of (u, d, s) quarks, then to $SU(4)_L \times SU(4)_R \times U(1)_A$ of (u, d, s, c) quarks, and finally to $SU(5)_L \times SU(5)_R \times U(1)_A$ of (u, d, s, c, b) quarks. This picture was first pointed out in Ref. [4]. Note that the t quark can be neglected in QCD since it is extremely short-lived and it decays to W-boson and quarks before it can interact with other quarks through the gluons. Moreover, since the QCD action with nonzero quark masses does not possess any chiral symmetries, “hierarchical restoration of chiral symmetry” should be regarded as “hierarchical emergence of chiral symmetry”.

In Ref. [5], the hierarchical restoration of chiral symmetry was first observed in $N_f = 2+1+1$ lattice QCD with (u, d, s, c) domain-wall quarks at the physical point, from $SU(2)_L \times SU(2)_R \times U(1)_A$ to $SU(3)_L \times SU(3)_R \times U(1)_A$, and then to $SU(4)_L \times SU(4)_R \times U(1)_A$, as the temperature is increased successively from 190 MeV to 1540 MeV. This confirms the picture of hierarchical restoration of chiral symmetry in QCD, but only partially, since the emergence of $SU(5)_L \times SU(5)_R \times U(1)_A$ of (u, d, s, c, b) quarks has not been verified. This motivates the present study to complete the picture of hierarchical restoration of chiral symmetry with $N_f = 2 + 1 + 1 + 1$ lattice QCD.

Nevertheless, it is a grand challenge to simulate $N_f = 2 + 1 + 1 + 1$ lattice QCD with (u, d, s, c, b) quarks at the physical point, as discussed in Ref. [6]. In order to have both discretization and finite volume errors under control, the constraints $a \lesssim 0.03$ fm and $M_\pi L > 4$ have to be satisfied, which impose the lattice size larger than $180^3 \times N_t$, beyond the present generation of lattice computations. Since our main goal is to observe the emergence of $SU(5)_L \times SU(5)_R \times U(1)_A$ in QCD with (u, d, s, c, b) quarks at $T \geq T_{c1}^{\bar{b}b} > T_{c1}^{\bar{c}c}$, after the chiral symmetry $SU(4)_L \times SU(4)_R \times U(1)_A$ of (u, d, s, c) quarks has been manifested at a lower temperature $T_{c1}^{\bar{c}c}$, we can address this problem in lattice QCD with physical (s, c, b) quarks but unphysical heavy u/d quarks (e.g., with $M_\pi \sim 700$ MeV). Then the simulation can be performed on $40^3 \times (64, 20, 16, 12, 10, 8, 6, 4, 2)$ lattices with a modest GPU cluster, where the ensemble of $40^3 \times 64$ lattice (at the “zero” temperature) has been generated in Ref. [6], together with the basic physical properties of mesons with quark contents $(\bar{b}b, \bar{b}c, \bar{b}s, \bar{c}c)$.

In this study, we generate the eight ensembles at finite temperatures, as summarized in I.

TABLE I: The lattice parameters and statistics of the eight gauge ensembles for computing the meson correlators. The HMC simulations are performed with the Wilson plaquette gauge action at $\beta = 6/g^2 = 6.70$, the two-flavor optimal domain-wall fermion action for u/d quarks, and the exact one-flavor optimal domain-wall fermion action for s, c , and b quarks. The lattice spacing $a = 0.0303(2)$ fm is determined by Wilson flow with the condition $\langle t^2 E(t) \rangle|_{t=t_0} = 0.3$, and input $\sqrt{t_0} = 0.1416(8)$ fm. The bare quark masses are $(m_{u/d}, m_s, m_c, m_b)a = (0.010, 0.015, 0.200, 0.850)$, where m_s, m_c and m_b are at the physical point, while the u/d quarks at the unphysical point with $M_\pi \sim 770$ MeV. The last four columns are the residual masses of $u/d, s, c$, and b quarks.

| N_x | N_t | $T[\text{MeV}]$ | N_{confs} | $(m_{u/d}a)_{\text{res}}$ | $(m_s a)_{\text{res}}$ | $(m_c a)_{\text{res}}$ | $(m_b a)_{\text{res}}$ |
|-------|-------|-----------------|--------------------|---------------------------|---------------------------|---------------------------|---------------------------|
| 40 | 20 | 325 | 306 | $8.21(33) \times 10^{-7}$ | $8.22(33) \times 10^{-7}$ | $8.70(33) \times 10^{-7}$ | $9.74(36) \times 10^{-7}$ |
| 40 | 16 | 406 | 382 | $9.35(28) \times 10^{-7}$ | $9.42(28) \times 10^{-7}$ | $9.82(28) \times 10^{-7}$ | $1.09(31) \times 10^{-6}$ |
| 40 | 12 | 524 | 380 | $9.46(28) \times 10^{-7}$ | $9.46(28) \times 10^{-7}$ | $9.74(28) \times 10^{-7}$ | $1.08(31) \times 10^{-7}$ |
| 40 | 10 | 650 | 260 | $9.12(33) \times 10^{-7}$ | $9.12(33) \times 10^{-7}$ | $9.25(34) \times 10^{-7}$ | $1.01(36) \times 10^{-8}$ |
| 40 | 8 | 813 | 337 | $1.03(3) \times 10^{-6}$ | $1.02(3) \times 10^{-6}$ | $1.04(3) \times 10^{-6}$ | $1.12(3) \times 10^{-6}$ |
| 40 | 6 | 1084 | 411 | $1.03(3) \times 10^{-6}$ | $1.03(3) \times 10^{-6}$ | $1.02(3) \times 10^{-6}$ | $1.07(3) \times 10^{-6}$ |
| 40 | 4 | 1626 | 337 | $1.13(4) \times 10^{-6}$ | $1.13(4) \times 10^{-6}$ | $1.12(4) \times 10^{-6}$ | $1.13(4) \times 10^{-6}$ |
| 40 | 2 | 3252 | 727 | $1.7(5) \times 10^{-7}$ | $1.7(5) \times 10^{-7}$ | $1.9(5) \times 10^{-7}$ | $2.3(5) \times 10^{-7}$ |

Details of the simulation algorithms, the determination of the lattice spacing a , the (s, c, b) physical quark masses, and the residual masses of $(u/d, s, c, b)$ quarks have been given in Ref. [6] and references therein.

Here we follow the same strategy of Refs. [4, 5] to use the splittings of the meson z -correlators of the symmetry multiplets to examine the realization of the hierarchical restoration of chiral symmetry in high temperature QCD. In general, the meson z -correlator $C_\Gamma(zT)$ of the meson interpolator $\bar{q}\Gamma Q$ is expressed as a function of the dimensionless variable

$$zT = (n_z a)/(N_t a) = n_z/N_t,$$

where $T = 1/(N_t a)$ is the temperature. For the classification of meson operators and their names and notations, see Table II in Ref. [5]. Moreover, we use the symmetry breaking

parameters as defined in Ref. [5], and follow the same conventions/notations therein. Here we also recall the notation

$$T_{c1}^{\bar{q}Q} \equiv \max(T_c^{\bar{q}Q}, T_1^{\bar{q}Q}), \quad (1)$$

where $T_c^{\bar{q}Q}$ ($T_1^{\bar{q}Q}$) is the temperature for the manifestation of $SU(2)_L \times SU(2)_R$ ($U(1)_A$) chiral symmetry via the meson z -correlators with flavor content $\bar{q}Q$. Then, for $T > T_{c1}^{\bar{q}Q}$, the theory possesses the $SU(2)_L \times SU(2)_R \times U(1)_A$ chiral symmetry of the $\bar{q}Q$ sector.

Besides the hierarchical restoration of chiral symmetry, we are also interested in the question whether there are any emergent symmetries which are not the symmetries of the entire QCD action but only a part of it, e.g., the $SU(2)_{CS}$ chiral-spin symmetry (with $U(1)_A$ as a subgroup) [7, 8], which is only a symmetry of chromoelectric part of the quark-gluon interaction, and also the color charge. Since the free fermions as well as the chromomagnetic part of the quark-gluon interaction do not possess the $SU(2)_{CS}$ symmetry, its emergence in high temperature QCD suggests the possible existence of hadronlike objects which are predominantly bound by chromoelectric interactions. The $SU(2)_{CS}$ symmetry was first observed to manifest approximately in the multiplets of z -correlators of vector mesons, at temperatures $T \sim 220 - 500$ MeV in $N_f = 2$ lattice QCD with domain-wall fermions [9]. In Ref. [4], we studied the emergence of $SU(2)_{CS}$ chiral-spin symmetry in $N_f = 2 + 1 + 1$ lattice QCD with optimal domain-wall quarks at the physical point, and found that the $SU(2)_{CS}$ symmetry breaking in the $\bar{u}d$ sector of $N_f = 2 + 1 + 1$ lattice QCD is larger than that in $N_f = 2$ lattice QCD at the same temperature, for both z -correlators and t -correlators of vector mesons of u and d quarks. In Ref. [5], we extended our study of $SU(2)_{CS}$ symmetry to all flavor combinations ($\bar{u}d$, $\bar{u}s$, $\bar{s}s$, $\bar{u}c$, $\bar{s}c$, $\bar{c}c$), and found that the T windows for the emergence of $SU(2)_{CS}$ symmetry are dominated by the ($\bar{u}c$, $\bar{s}c$, $\bar{c}c$) sectors. In this work, we extend our study to $N_f = 2 + 1 + 1 + 1$ lattice QCD with physical (s, c, b) but unphysically heavy u/d (with $M_\pi \sim 700$ MeV).

The outline of this paper is as follows. In Sec. II, we demonstrate the realization of the hierarchical restoration of chiral symmetry in $N_f = 2 + 1 + 1 + 1$ QCD, from $SU(2)_L \times SU(2)_R \times U(1)_A$ to $SU(3)_L \times SU(3)_R \times U(1)_A$, then to $SU(4)_L \times SU(4)_R \times U(1)_A$, and finally to $SU(5)_L \times SU(5)_R \times U(1)_A$. In Sec. III, the temperature windows for the $SU(2)_{CS}$ symmetry of ten flavor combinations are obtained. They reveal that the $SU(2)_{CS}$ symmetry

is dominated by the $(\bar{u}b, \bar{s}b)$ sectors. In Sec. IV, we conclude with some remarks.

II. Hierarchical restoration of chiral symmetry

First, we recall the $SU(2)_L \times SU(2)_R$ and $U(1)$ symmetry breaking parameters as defined in Ref. [5].

The $SU(2)_L \times SU(2)_R$ symmetry breaking for any $\bar{q}Q$ sector can be measured by

$$\kappa_{VA}(zT) = \frac{|C_{V_k}(zT) - C_{A_k}(zT)|}{C_{V_k}(zT) + C_{A_k}(zT)}, \quad z > 0, \quad (k = 1, 2, 4). \quad (2)$$

In the following, we use (2) with $k = 1$ to measure the $SU(2)_L \times SU(2)_R$ symmetry breaking.

In general, to determine to what extent the $SU(2)_L \times SU(2)_R$ chiral symmetry is manifested, it is necessary to examine whether κ_{VA} is sufficiently small. To this end, we use the following criterion for the manifestation of $SU(2)_L \times SU(2)_R$ chiral symmetry at T for a fixed zT ,

$$\kappa_{VA}(zT) \leq \epsilon_{VA}, \quad (3)$$

where ϵ_{VA} is a small parameter which defines the precision of the chiral symmetry. For fixed zT and ϵ_{VA} , the temperature T_c is the lowest temperature satisfying (3), i.e.,

$$\kappa_{VA}(zT) < \epsilon_{VA} \text{ for } T > T_c. \quad (4)$$

In this study, we set ϵ_{VA} to three different values, 0.01, 0.005 and 0.001, to examine how T_c depends on ϵ_{VA} .

The $U(1)_A$ symmetry breaking for any $\bar{q}Q$ sector can be measured by the z -correlators in the pseudoscalar and scalar channels, with

$$\kappa_{PS}(zT) = \frac{|C_P(zT) - C_S(zT)|}{C_P(zT) + C_S(zT)}, \quad z > 0,$$

as well as in the tensor vector and axial-tensor vector channels, with

$$\kappa_{TX}(zT) = \frac{|C_{T_k}(zT) - C_{X_k}(zT)|}{C_{T_k}(zT) + C_{X_k}(zT)}, \quad z > 0, \quad (k = 1, 2, 4). \quad (5)$$

In the following, we use (5) with $k = 4$ to measure the $U(1)_A$ symmetry breaking.

Similar to (3), we use the following criterion for the manifestation of $U(1)_A$ symmetry at T for a fixed zT

$$\kappa_{TX}(zT) \leq \epsilon_{TX}, \quad (6)$$

where ϵ_{TX} is a small parameter which defines the precision of $U(1)_A$ symmetry. For fixed zT and ϵ_{TX} , the temperature T_1 is the lowest temperature satisfying (6), i.e.,

$$\kappa_{TX}(zT) < \epsilon_{TX} \text{ for } T > T_1. \quad (7)$$

In this study, we set ϵ_{TX} to three different values, 0.01, 0.005 and 0.001, to examine how T_1 depends on ϵ_{TX} .

Next, consider QCD with $N_f \geq 2$ quarks $(q_1, q_2, \dots, q_{N_f})$. As discussed in Ref. [5], upon neglecting the disconnected diagrams in the meson z -correlators, the $SU(N)_L \times SU(N)_R$ chiral symmetry of N ($2 \leq N \leq N_f$) quarks is manifested by the degeneracies of meson z -correlators in the vector and axial-vector channels, $C_{V_k}^{\bar{q}_i q_j}(z) = C_{A_k}^{\bar{q}_i q_j}(z)$, ($k = 1, 2, 4$), for *all* flavor combinations of N quarks $(\bar{q}_i q_j, i, j = 1, \dots, N)$. Thus, to determine the temperature T_c for the manifestation of the $SU(N)_L \times SU(N)_R$ chiral symmetry of N quarks, it needs to measure $\kappa_{VA}^{\bar{q}_i q_j}$ for *all* flavor combinations of N quarks, and check whether they *all* satisfy the criterion (3) for fixed zT and ϵ_{VA} . This amounts to finding the largest $T_c^{\bar{q}_i q_j}$ satisfying (3) among all flavor combinations of N quarks, i.e.,

$$T_c = \max(T_c^{\bar{q}_i q_j}, i, j = 1, 2, \dots, N). \quad (8)$$

Similarly, about the $U(1)_A$ symmetry of N ($2 \leq N \leq N_f$) quarks, upon neglecting the disconnected diagrams in the meson z -correlators, it is manifested by the degeneracies of meson z -correlators in the pseudoscalar and scalar channels, $C_P^{\bar{q}_i q_j}(z) = C_S^{\bar{q}_i q_j}(z)$, as well as in the tensor vector and axial-tensor vector channels, $C_{T_k}^{\bar{q}_i q_j}(z) = C_{X_k}^{\bar{q}_i q_j}(z)$, ($k = 1, 2, 4$), for *all* flavor combinations of N quarks $(\bar{q}_i q_j, i, j = 1, \dots, N)$. To determine the temperature T_1 for the manifestation of $U(1)_A$ symmetry via the $k = 4$ component of the tensor vector and axial-tensor vector channels, it needs to measure $\kappa_{TX}^{\bar{q}_i q_j}$ for *all* flavor combinations of N quarks, and check whether they *all* satisfy the criterion (6) for fixed zT and ϵ_{TX} . This amounts to finding the largest $T_1^{\bar{q}_i q_j}$ satisfying (6) among all flavor combinations of N quarks, i.e.,

$$T_1 = \max(T_1^{\bar{q}_i q_j}, i, j = 1, 2, \dots, N). \quad (9)$$

At this point, we recall that the meson z -correlators of the flavor singlet and the flavor nonsinglet of the same quantum number (i.e., scalar, pseudoscalar, tensor vector, or axial-tensor vector) are equal at $T > T_c$ for QCD with $N_f > 2$ massless quarks [10–12]. This implies that at $T > T_c$ the disconnected diagrams are suppressed in meson z -correlators for QCD with $N_f > 2$ massless quarks. However, it is unknown to what extent the disconnected diagrams are suppressed in QCD with $N_f = 2 + 1 + 1 + 1$ massive quarks. We will address this question with noise estimation of all-to-all quark propagators, which is now underway.

FIG. 1: The chiral symmetry breaking parameters (κ_{VA}, κ_{TX}) of ($\bar{u}d, \bar{u}s, \bar{s}s$) mesons.

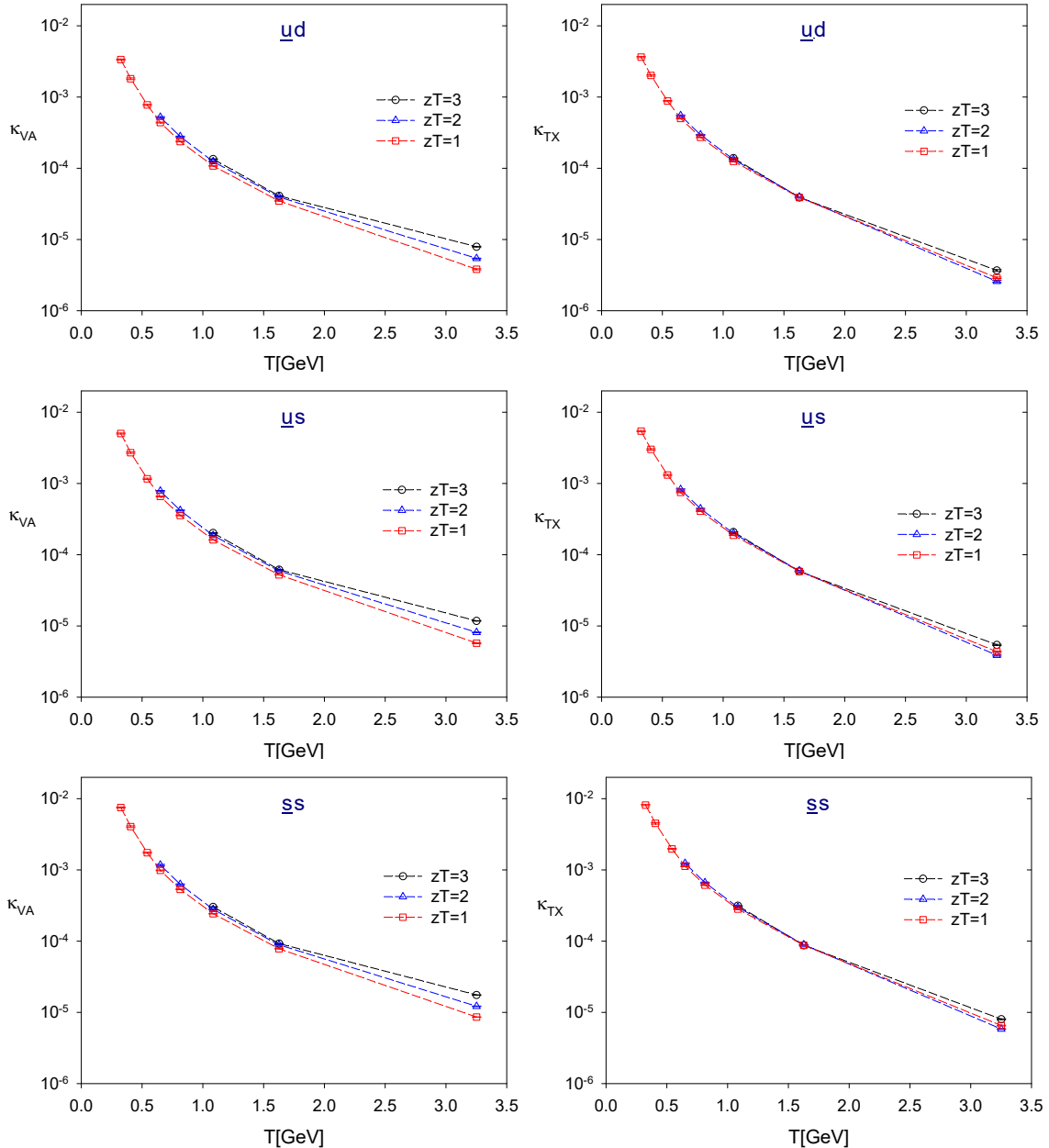


FIG. 2: The chiral symmetry breaking parameters (κ_{VA}, κ_{TX}) of ($\bar{u}c, \bar{s}c, \bar{u}b, \bar{s}b$) mesons.

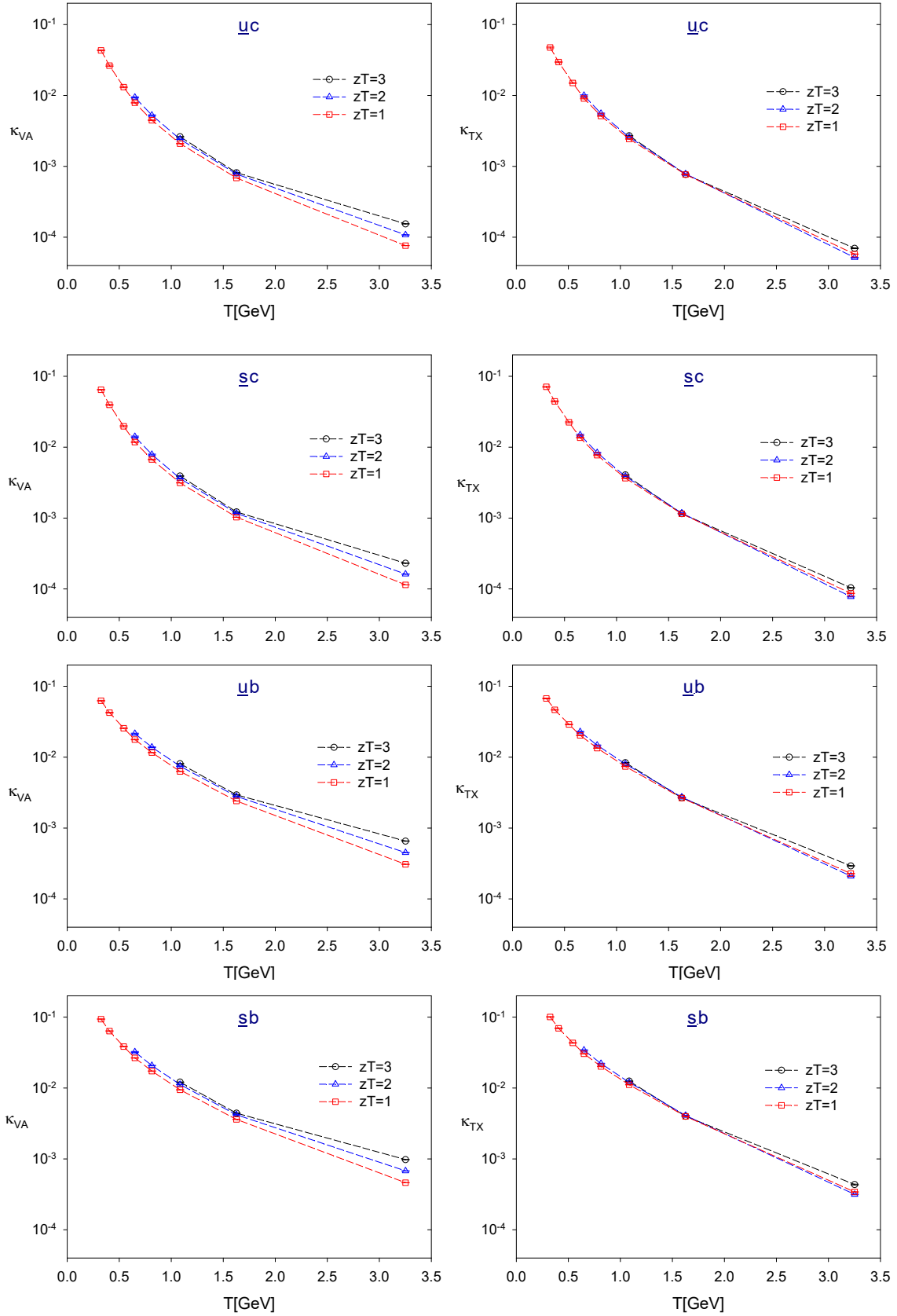
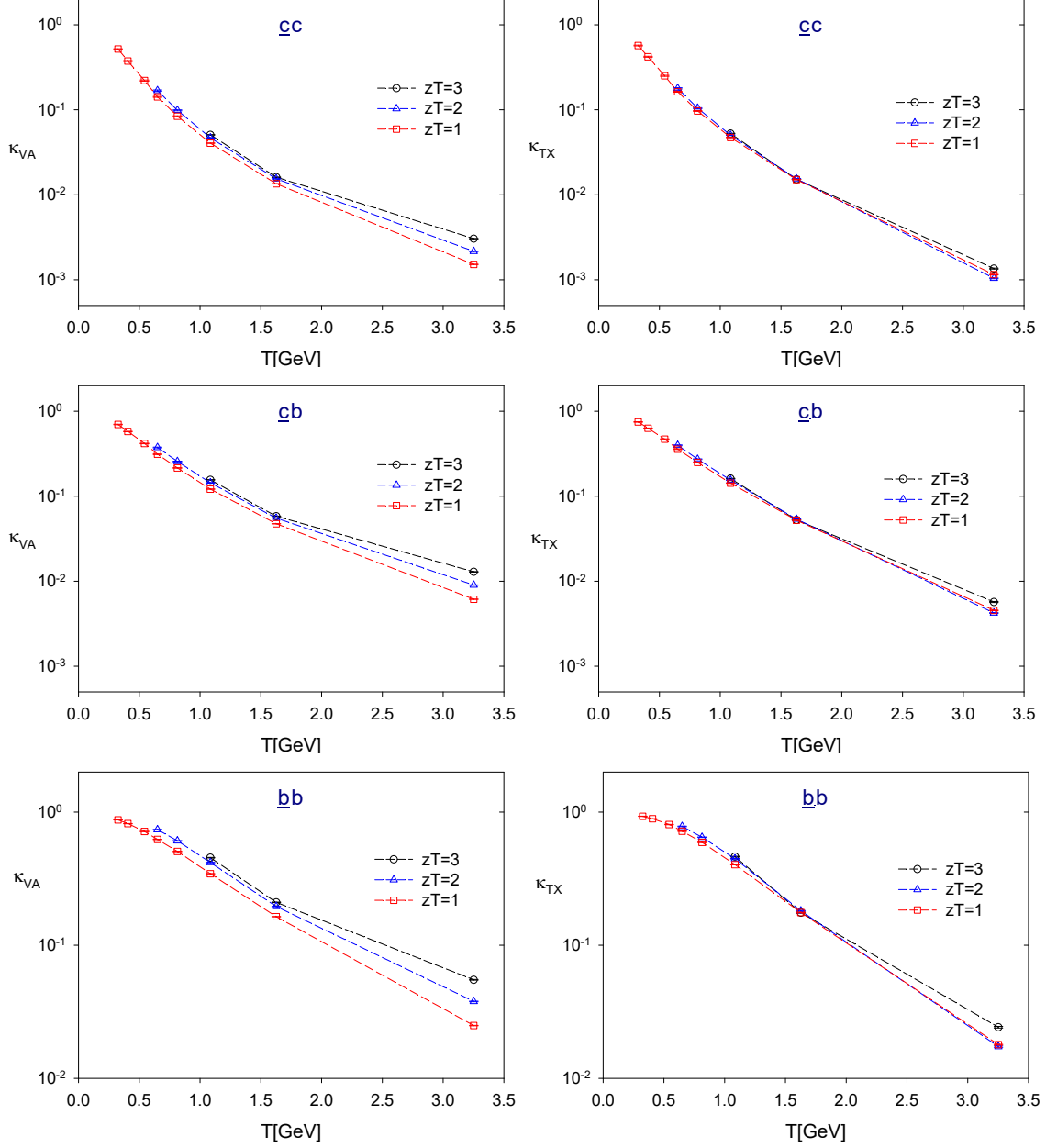


FIG. 3: The chiral symmetry breaking parameters (κ_{VA}, κ_{TX}) of ($\bar{c}c, \bar{c}b, \bar{b}b$) mesons.



Now we proceed to investigate the hierarchical restoration of chiral symmetry in $N_f = 2 + 1 + 1 + 1$ lattice QCD with physical s , c and b quarks but unphysically heavy u/d quarks (with $M_\pi \sim 700$ MeV). We use the criteria (3) and (6) to obtain T_c and T_1 for each flavor combination. To this end, we compute $\kappa_{VA}(zT)$ and $\kappa_{TX}(zT)$ and plot them as a function of T , for $zT = (1, 2, 3)$, as shown in Figs. 1-3.

At each T , and for fixed zT , the chiral symmetry breakings due to the quark masses of the meson operator can be seen clearly from κ_{VA} and κ_{TX} , in the order of

$$\kappa_{\alpha}^{\bar{u}d} < \kappa_{\alpha}^{\bar{u}s} < \kappa_{\alpha}^{\bar{s}s} < \kappa_{\alpha}^{\bar{u}c} < \kappa_{\alpha}^{\bar{s}c} < \kappa_{\alpha}^{\bar{u}b} < \kappa_{\alpha}^{\bar{s}b} < \kappa_{\alpha}^{\bar{c}c} < \kappa_{\alpha}^{\bar{c}b} < \kappa_{\alpha}^{\bar{b}b}, \quad (10)$$

where $\alpha = VA, TX$. Also, for each flavor content, $\kappa_{\alpha}(zT)$ at fixed zT is a monotonic decreasing function of T . It follows that for any ϵ_{VA} in (3) and any ϵ_{TX} in (6), the flavor dependence of T_c and T_1 is in the order of

$$T_c^{\bar{u}d} < T_c^{\bar{u}s} < T_c^{\bar{s}s} < T_c^{\bar{u}c} < T_c^{\bar{s}c} < T_c^{\bar{u}b} < T_c^{\bar{s}b} < T_c^{\bar{c}c} < T_c^{\bar{c}b} < T_c^{\bar{b}b}, \quad (11)$$

$$T_1^{\bar{u}d} < T_1^{\bar{u}s} < T_1^{\bar{s}s} < T_1^{\bar{u}c} < T_1^{\bar{s}c} < T_1^{\bar{u}b} < T_1^{\bar{s}b} < T_1^{\bar{c}c} < T_1^{\bar{c}b} < T_1^{\bar{b}b}. \quad (12)$$

This immediately gives

$$T_{c1}^{\bar{u}d} < T_{c1}^{\bar{u}s} < T_{c1}^{\bar{s}s} < T_{c1}^{\bar{u}c} < T_{c1}^{\bar{s}c} < T_{c1}^{\bar{u}b} < T_{c1}^{\bar{s}b} < T_{c1}^{\bar{c}c} < T_{c1}^{\bar{c}b} < T_{c1}^{\bar{b}b}, \quad (13)$$

and the hierarachic restoration of chiral symmetry in $N_f = 2 + 1 + 1 + 1$ QCD, i.e., from the restoration of $SU(2)_L \times SU(2)_R \times U(1)_A$ chiral symmetry of (u, d) quarks at $T > T_{c1}^{\bar{u}d}$ to the the restoration of $SU(3)_L \times SU(3)_R \times U(1)_A$ chiral symmetry of (u, d, s) quarks at $T > T_{c1}^{\bar{s}s}$, then to the restoration of $SU(4)_L \times SU(4)_R \times U(1)_A$ chiral symmetry of (u, d, s, c) quarks at $T > T_{c1}^{\bar{c}c}$, and finally to $SU(5)_L \times SU(5)_R \times U(1)_A$ chiral symmetry of (u, d, s, c, b) quarks at $T > T_{c1}^{\bar{b}b}$.

In the following, we demonstrate the hierarchical restoration of chiral symmetry explicitly, for $\epsilon_{VA} = (0.01, 0.005, 0.001)$ and $\epsilon_{TX} = (0.01, 0.005, 0.001)$ respectively.

Using the data points in each figure of Figs. 1-3 for interpolation/extrapolation, we obtain the results of T_c and T_1 for ten flavor combinations, as listed in Tables II and III, for $\epsilon_{VA} = (0.010, 0.0050, 0.0010)$ and $\epsilon_{TX} = (0.010, 0.0050, 0.0010)$ respectively.

TABLE II: The temperature $T_c^{\bar{q}_1 q_2}$ [MeV] satisfying the criterion (3) at $zT = (1, 2, 3)$, for $\epsilon_{VA} = (0.01, 0.005, 0.001)$ respectively.

| | $zT = 1$ | | | $zT = 2$ | | | $zT = 3$ | | |
|------------------|----------|----------|----------|----------|----------|----------|----------|----------|----------|
| ϵ_{VA} | 0.01 | 0.005 | 0.001 | 0.01 | 0.005 | 0.001 | 0.01 | 0.005 | 0.001 |
| $T_c^{\bar{u}d}$ | 182(8) | 273(9) | 501(11) | 210(16) | 302(18) | 530(16) | 230(16) | 310(20) | 542(18) |
| $T_c^{\bar{u}s}$ | 234(8) | 325(10) | 570(9) | 255(14) | 344(16) | 586(12) | 276(17) | 346(22) | 600(30) |
| $T_c^{\bar{s}s}$ | 310(9) | 378(10) | 647(7) | 331(12) | 427(17) | 691(10) | 366(13) | 458(20) | 722(22) |
| $T_c^{\bar{u}c}$ | 599(8) | 780(11) | 1442(6) | 632(15) | 830(11) | 1505(9) | 656(14) | 857(23) | 1529(9) |
| $T_c^{\bar{s}c}$ | 697(8) | 917(12) | 1646(6) | 746(9) | 971(8) | 1753(10) | 762(12) | 970(10) | 1818(10) |
| $T_c^{\bar{u}b}$ | 878(10) | 1213(8) | 2320(10) | 954(13) | 1304(14) | 2540(10) | 982(10) | 1341(10) | 2793(12) |
| $T_c^{\bar{s}b}$ | 1057(11) | 1442(7) | 2641(10) | 1146(11) | 1528(10) | 2902(12) | 1186(9) | 1158(10) | 3228(16) |
| $T_c^{\bar{c}c}$ | 1849(14) | 2365(12) | 3563(10) | 1983(8) | 2557(10) | 3889(11) | 2091(11) | 2768(14) | 4342(16) |
| $T_c^{\bar{c}b}$ | 2864(12) | 3415(10) | 4696(10) | 3159(10) | 3781(12) | 5226(14) | 3527(16) | 4276(16) | 6014(20) |
| $T_c^{\bar{b}b}$ | 4039(10) | 4637(12) | 6026(12) | 4568(10) | 5255(21) | 6849(27) | 5321(20) | 6163(24) | 8117(28) |

TABLE III: The temperature $T_1^{\bar{q}_1 q_2}$ [MeV] satisfying the criterion (6) at $zT = (1, 2, 3)$, for $\epsilon_{TX} = (0.01, 0.005, 0.001)$ respectively.

| | $zT = 1$ | | | $zT = 2$ | | | $zT = 3$ | | |
|------------------|----------|----------|----------|----------|----------|----------|----------|----------|----------|
| ϵ_{TX} | 0.01 | 0.005 | 0.001 | 0.01 | 0.005 | 0.001 | 0.01 | 0.005 | 0.001 |
| $T_1^{\bar{u}d}$ | 187(5) | 281(7) | 520(6) | 201(12) | 295(16) | 544(14) | 210(21) | 305(18) | 551(17) |
| $T_1^{\bar{u}s}$ | 241(6) | 336(6) | 594(8) | 248(10) | 340(14) | 600(12) | 262(13) | 357(17) | 616(12) |
| $T_1^{\bar{s}s}$ | 315(7) | 392(8) | 681(8) | 334(14) | 425(14) | 705(10) | 354(19) | 446(22) | 728(18) |
| $T_1^{\bar{u}c}$ | 628(6) | 822(9) | 1501(10) | 650(10) | 850(10) | 1514(8) | 665(12) | 877(16) | 1512(23) |
| $T_1^{\bar{s}c}$ | 738(10) | 969(8) | 1713(11) | 761(8) | 993(8) | 1721(8) | 794(15) | 994(11) | 1721(10) |
| $T_1^{\bar{u}b}$ | 945(8) | 1290(8) | 2272(11) | 984(8) | 1321(8) | 2261(10) | 999(13) | 1327(10) | 2347(16) |
| $T_1^{\bar{s}b}$ | 1139(9) | 1505(8) | 2540(12) | 1175(10) | 1525(10) | 2520(12) | 1190(11) | 1519(12) | 2641(16) |
| $T_1^{\bar{c}c}$ | 1886(12) | 2324(10) | 3341(13) | 1886(8) | 2305(14) | 3277(16) | 1907(10) | 2373(12) | 3456(20) |
| $T_1^{\bar{c}b}$ | 2726(10) | 3187(10) | 4259(12) | 2701(12) | 3145(14) | 4174(20) | 2840(16) | 3347(23) | 4525(35) |
| $T_1^{\bar{b}b}$ | 3666(12) | 4159(14) | 5305(24) | 3631(20) | 4111(24) | 5224(20) | 3977(27) | 4546(32) | 5867(55) |

Now we demonstrate the hierarchical restoration of chiral symmetry with $\epsilon_{VA} = \epsilon_{TX} = 0.01$ and $zT = 1$, according to the first column of the $zT = 1$ section in Tables II-III. For the $\bar{u}d$ sector, $T_c^{\bar{u}d} \sim 182$ MeV and $T_1^{\bar{u}d} \sim 187$ MeV. Thus the $SU(2)_L \times SU(2)_R \times U(1)_A$ chiral symmetry of (u, d) is restored at $T_{c1}^{\bar{u}d} \sim 187$ MeV. Since the u/d quarks are unphysically heavy in this study, the physical $T_{c1}^{\bar{u}d}$ must be lower than 187 MeV. Next, for the $\bar{s}s$ sector, $T_c^{\bar{s}s} \sim 310$ MeV and $T_1^{\bar{s}s} \sim 315$ MeV, and both are higher than those of $\bar{u}s$ and $\bar{u}d$ sectors. Thus the $SU(3)_L \times SU(3)_R \times U(1)_A$ chiral symmetry of (u, d, s) quarks is restored at $T_{c1}^{\bar{s}s} \sim 315$ MeV. Next, for the $\bar{c}c$ sector, $T_c^{\bar{c}c} \sim 1850$ MeV and $T_1^{\bar{c}c} \sim 1885$ MeV, and both are higher than those of $(\bar{u}d, \bar{u}s, \bar{s}s, \bar{u}c, \bar{s}c)$ sectors, in the order of (11) and (12). Thus the $SU(4)_L \times SU(4)_R \times U(1)_A$ chiral symmetry of (u, d, s, c) quarks is restored at $T_{c1}^{\bar{c}c} \sim 1885$ MeV. Finally, for the $\bar{b}b$ sector, $T_c^{\bar{b}b} \sim 4040$ MeV and $T_1^{\bar{b}b} \sim 3670$ MeV, and both are higher than those of all other sectors, thus the $SU(5)_L \times SU(5)_R \times U(1)_A$ chiral symmetry of (u, d, s, c, b) quarks is restored at $T_{c1}^{\bar{b}b} \sim 4040$ MeV.

At this point, we compare the values of $T_{c1}^{\bar{s}s}$ and $T_{c1}^{\bar{c}c}$ with those in $N_f = 2 + 1 + 1$ lattice QCD at the physical point [5]. For example, at $zT = 1$ and $\epsilon_{VA} = \epsilon_{TX} = 0.01$, we have the results in Table IV.

TABLE IV: Comparison of $T_{c1}^{\bar{s}s}$ and $T_{c1}^{\bar{c}c}$ between $N_f = 2 + 1 + 1$ and $N_f = 2 + 1 + 1 + 1$ lattice QCD, at $zT = 1$ and $\epsilon_{VA} = \epsilon_{TX} = 0.01$.

| | $N_f = 2 + 1 + 1$ [5] | $N_f = 2 + 1 + 1 + 1$ (this work) |
|---------------------|-----------------------|-----------------------------------|
| $T_{c1}^{\bar{s}s}$ | 320(5) MeV | 315(7) MeV |
| $T_{c1}^{\bar{c}c}$ | 1395(5) MeV | 1886(12) MeV |

The $T_{c1}^{\bar{s}s}$ values in $N_f = 2 + 1 + 1 + 1$ QCD (this work) and $N_f = 2 + 1 + 1$ QCD at the physical point [5] agree well. However, the $T_{c1}^{\bar{c}c}$ in $N_f = 2 + 1 + 1 + 1$ QCD is over 400 MeV higher than that in $N_f = 2 + 1 + 1$ QCD. The causes leading to the discrepancy are unclear, which may be due to systematic errors, such as the unphysically heavy u/d quarks in this study, the absence of dynamical b quark in $N_f = 2 + 1 + 1$ QCD [5], and different discretization errors (with $a \approx 0.030$ fm in this work versus $a \approx 0.064$ fm in [5]).

Next, we study how T_c (T_1) depends on ϵ_{VA} (ϵ_{TX}). Since $\kappa_{VA}^{\bar{q}_1 q_2} (\kappa_{TX}^{\bar{q}_1 q_2})$ at fixed zT is a monotonic decreasing function of T , it follows that T_c (T_1) is monotonically increased as ϵ_{VA}

(ϵ_{TX}) is decreased (i.e., the precision of the chiral symmetry becomes higher). For example, consider at $zT = 1$, both ϵ_{VA} and ϵ_{TX} are decreased from 0.01 to 0.005. According to the second column of the $zT = 1$ section in Tables II-III, it is straightforward to obtain the following results. First, the $SU(2)_L \times SU(2)_R \times U(1)_A$ chiral symmetry of (u, d) quarks is restored at $T_{c1}^{\bar{u}d} \sim 280$ MeV (since $T_c^{\bar{u}d} \sim 275$ MeV and $T_1^{\bar{u}d} \sim 280$ MeV). Next, the $SU(3)_L \times SU(3)_R \times U(1)_A$ chiral symmetry of (u, d, s) quarks is restored at $T_{c1}^{\bar{s}s} \sim 390$ MeV (since $T_c^{\bar{s}s} \sim 380$ MeV and $T_1^{\bar{s}s} \sim 390$ MeV). Then, the $SU(4)_L \times SU(4)_R \times U(1)_A$ chiral symmetry of (u, d, s, c) quarks is restored at $T_{c1}^{\bar{c}c} \sim 2370$ MeV (since $T_c^{\bar{c}c} \sim 2370$ MeV and $T_1^{\bar{c}c} \sim 2325$ MeV). Finally, the $SU(5)_L \times SU(5)_R \times U(1)_A$ chiral symmetry of (u, d, s, c, b) quarks is restored at $T_{c1}^{\bar{b}b} \sim 4640$ MeV (since $T_c^{\bar{b}b} \sim 4640$ MeV and $T_1^{\bar{b}b} \sim 4160$ MeV). Obviously, no matter how small the values of ϵ_{VA} and ϵ_{TX} become, the hierarchical restoration of chiral symmetry in QCD with (u, d, s, c, b) quarks will occur at higher temperatures.

III. $SU(2)_{CS}$ chiral-spin symmetry

First, we recall the SU_{CS} symmetry breaking and fading parameters (κ_{CS}, κ) as defined in Ref. [5].

In general, to examine the emergence of $SU(2)_{CS}$ symmetry, it needs to measure the splittings in the $SU_{CS}(2)$ multiplet (A_1, T_4, X_4) . Since the splitting of T_4 and X_4 has been measured by the $U(1)_A$ symmetry breaking parameter κ_{TX} (5) with $k = 4$, it remains to measure the splitting of A_1 and X_4 with

$$\kappa_{AX}(zT) = \frac{|C_{A_1}(zT) - C_{X_4}(zT)|}{C_{A_1}(zT) + C_{X_4}(zT)}, \quad z > 0, \quad (14)$$

then taking the maximum of κ_{AT} and κ_{TX} as the $SU(2)_{CS}$ symmetry breaking parameter,

$$\kappa_{CS} = \max(\kappa_{AX}, \kappa_{TX}). \quad (15)$$

Note that κ_{AX} in (14) is exactly the same as κ_{AT} in Ref. [5]. Here we just change the subscript from AT to AX for consistency, since it refers to the splitting of the axial vector A_1 and the axial-tensor vector X_4 .

As the temperature T is increased, the separation between the multiplets of $SU(2)_{CS}$ and $U(1)_A$ is decreased. Therefore, at sufficiently high temperatures $T > T_c^{\bar{q}Q}$, the $U(1)_A$ multiplet $M_0 = (P, S)$ and the $SU(2)_{CS} \times SU(2)_L \times SU(2)_R$ multiplet $M_2 = (V_1, A_1, T_4, X_4)$

merge together, then the $SU(2)_{CS}$ symmetry becomes washed out, and only the $SU(2)_L \times SU(2)_R \times U(1)_A$ chiral symmetry remains. Following Ref. [5], We use $\kappa(zT)$ to measure the fading of the $SU(2)_{CS}$ symmetry.

$$\kappa(zT) = \left| \frac{C_{A_1}(zT) - C_{X_4}(zT)}{C_{M_0}(zT) - C_{M_2}(zT)} \right|, \quad z > 0, \quad (16)$$

where

$$C_{M_0}(zT) \equiv \frac{1}{2} [C_P(zT) + C_S(zT)],$$

$$C_{M_2}(zT) \equiv \frac{1}{4} [C_{V_1}(zT) + C_{A_1}(zT) + C_{T_4}(zT) + C_{X_4}(zT)].$$

Thus, to determine to what extent the $SU(2)_{CS}$ symmetry is manifested in the z -correlators, it is necessary to examine whether both $\kappa(zT)$ and $\kappa_{CS}(zT)$ are sufficiently small. For a fixed zT , the following condition

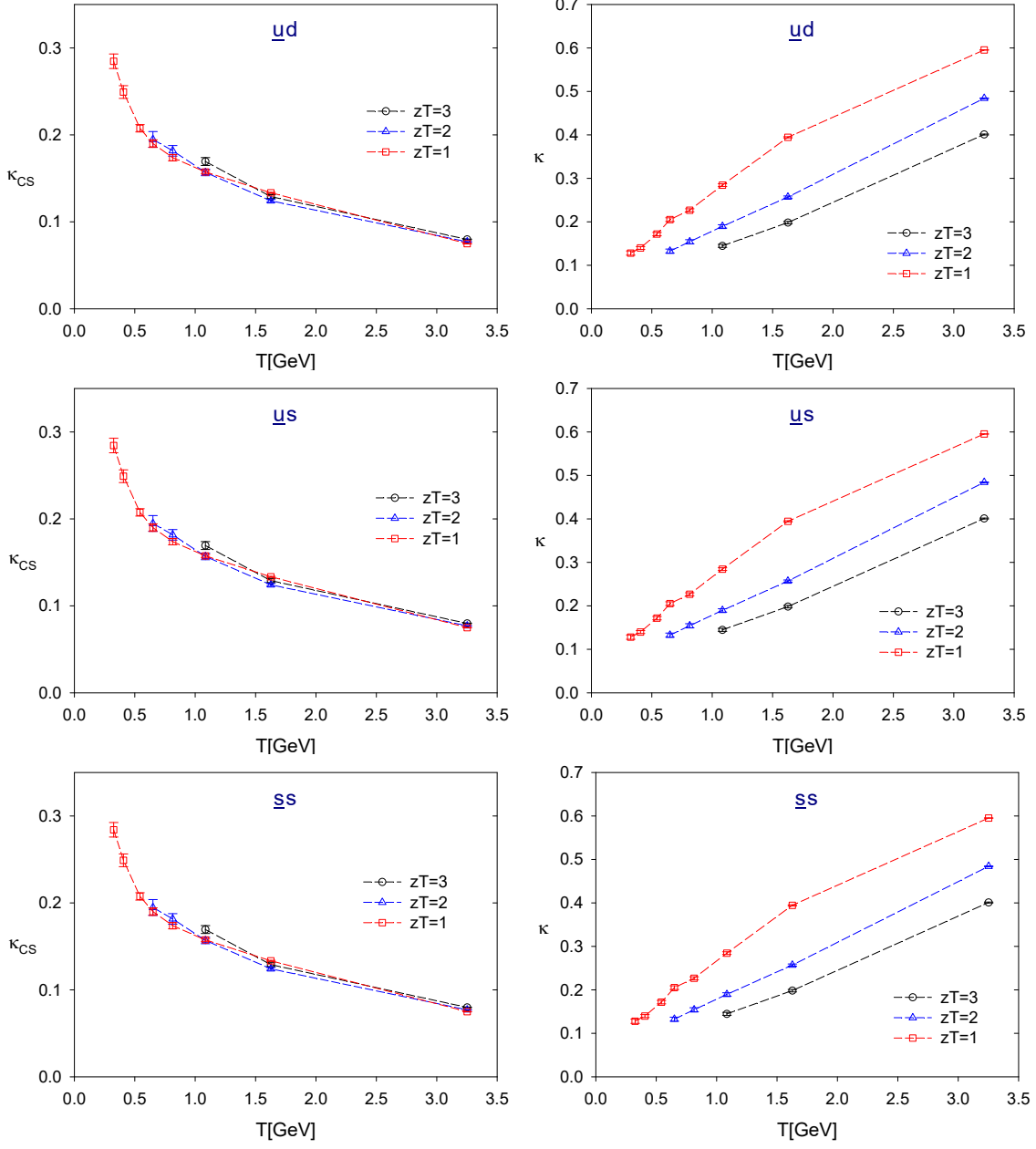
$$(\kappa_{CS}(zT) < \epsilon_{cs}) \wedge (\kappa(zT) < \epsilon_{fcs}) \quad (17)$$

serves as a criterion for the $SU(2)_{CS}$ symmetry in the z -correlators, where ϵ_{cs} is for the $SU(2)_{CS}$ symmetry breaking, while ϵ_{fcs} for the $SU(2)_{CS}$ symmetry fading. For fixed zT , (17) gives a window of T for the $SU(2)_{CS}$ symmetry. Obviously, the size of this window depends on ϵ_{cs} and ϵ_{fcs} . That is, larger ϵ_{cs} or ϵ_{fcs} gives a wider window of T , and conversely, smaller ϵ_{cs} or ϵ_{fcs} gives a narrower window of T .

Next we proceed to study the $SU(2)_{CS}$ symmetry of $N_f = 2 + 1 + 1 + 1$ lattice QCD with physical s , c , and b , but unphysically heavy u/d (with $M_\pi \sim 700$ MeV). We use the criterion (17) to determine the window of T of the $SU(2)_{CS}$ symmetry, for ten flavor combinations. To this end, we collect the data of $SU(2)_{CS}$ symmetry-breaking parameter $\kappa_{CS} = \max(\kappa_{AX}, \kappa_{TX})$ and symmetry-fading parameter κ at $zT = (2, 3)$, and plot them as a function of T , in Figs. 4-6, for vector mesons with flavor contents $(\bar{u}d, \bar{u}s, \bar{s}s)$, $(\bar{u}c, \bar{s}c, \bar{u}b, \bar{s}b)$, and $(\bar{c}c, \bar{c}b, \bar{b}b)$ respectively.

Note that for the $(\bar{u}d, \bar{u}s, \bar{s}s, \bar{u}c, \bar{s}c, \bar{u}b, \bar{s}b)$ sectors, $\kappa_{AX}(zT) > \kappa_{TX}(zT)$ for any zT at the same T , thus $\kappa_{CS} = \kappa_{AX}$. On the other hand, for the $(\bar{c}c, \bar{c}b, \bar{b}b)$ sectors, $\kappa_{AX}(zT) < \kappa_{TX}(zT)$ at low temperatures, thus κ_{CS} has an abrupt change at some temperature between low and high temperatures, which can be seen from the left panels in Fig. 6.

FIG. 4: The chiral-spin symmetry breaking and fading parameters of $(\bar{u}d, \bar{u}s, \bar{s}s)$ vector mesons.



In general, for any flavor content, at fixed zT , κ is a monotonic increasing function of T , while κ_{CS} is a monotonic decreasing function of T except for the $\bar{u}b$ and $\bar{s}b$ sectors as shown in Fig. 5. Thus, for any ϵ_{cs} and ϵ_{fcs} , the window of T satisfying the criterion (17) can be determined for any flavor content. Moreover, when ϵ_{cs} or ϵ_{fcs} becomes too small, the window of T would shrink to zero (null). Using interpolation/extrapolation of the data points in Figs. 4-6, we obtain the T windows in Tables V-VI at $zT = (2, 3)$ respectively, each for ten

FIG. 5: The chiral-spin symmetry breaking and fading parameters of $(\bar{u}c, \bar{s}c, \bar{s}c, \bar{s}b)$ mesons.

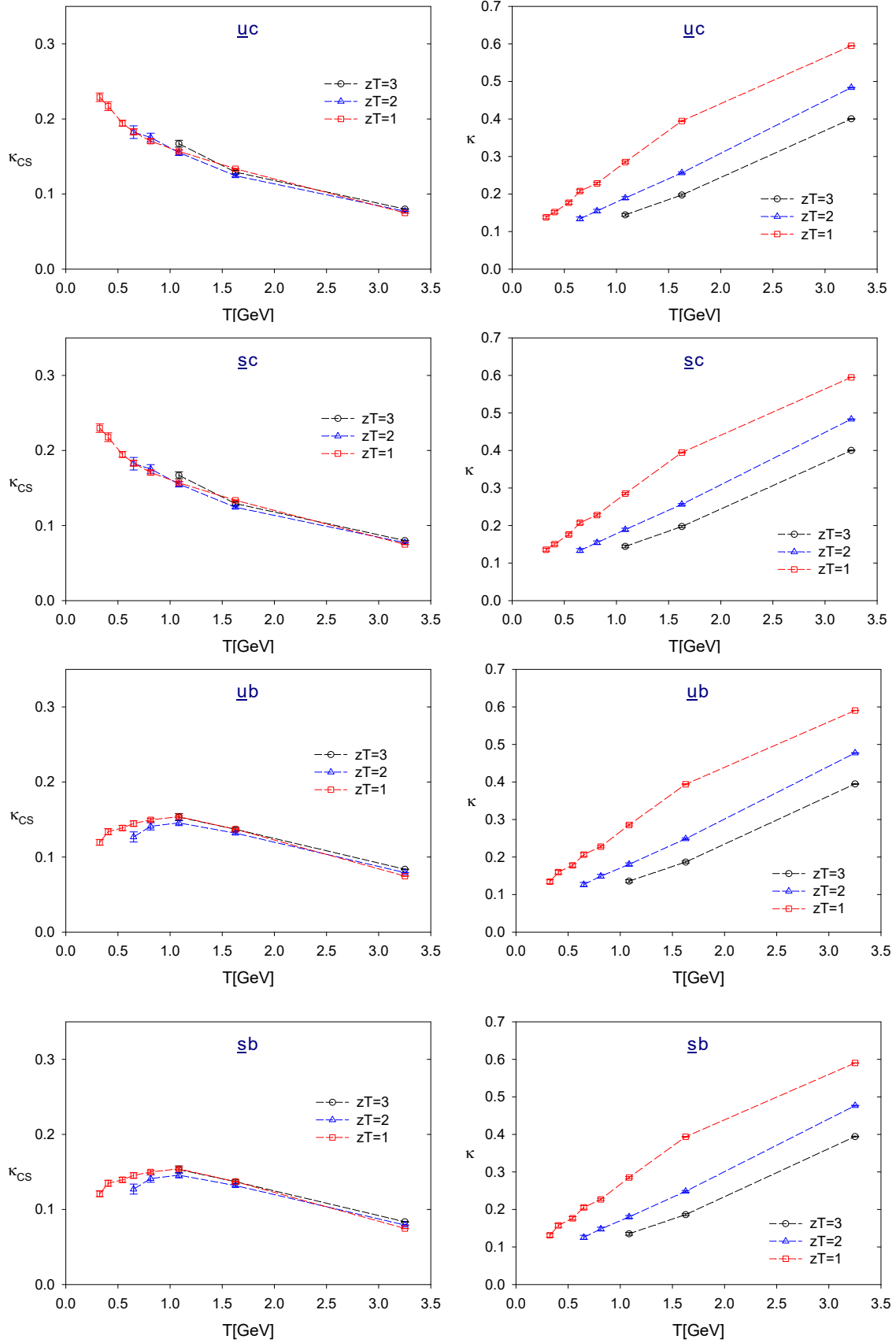
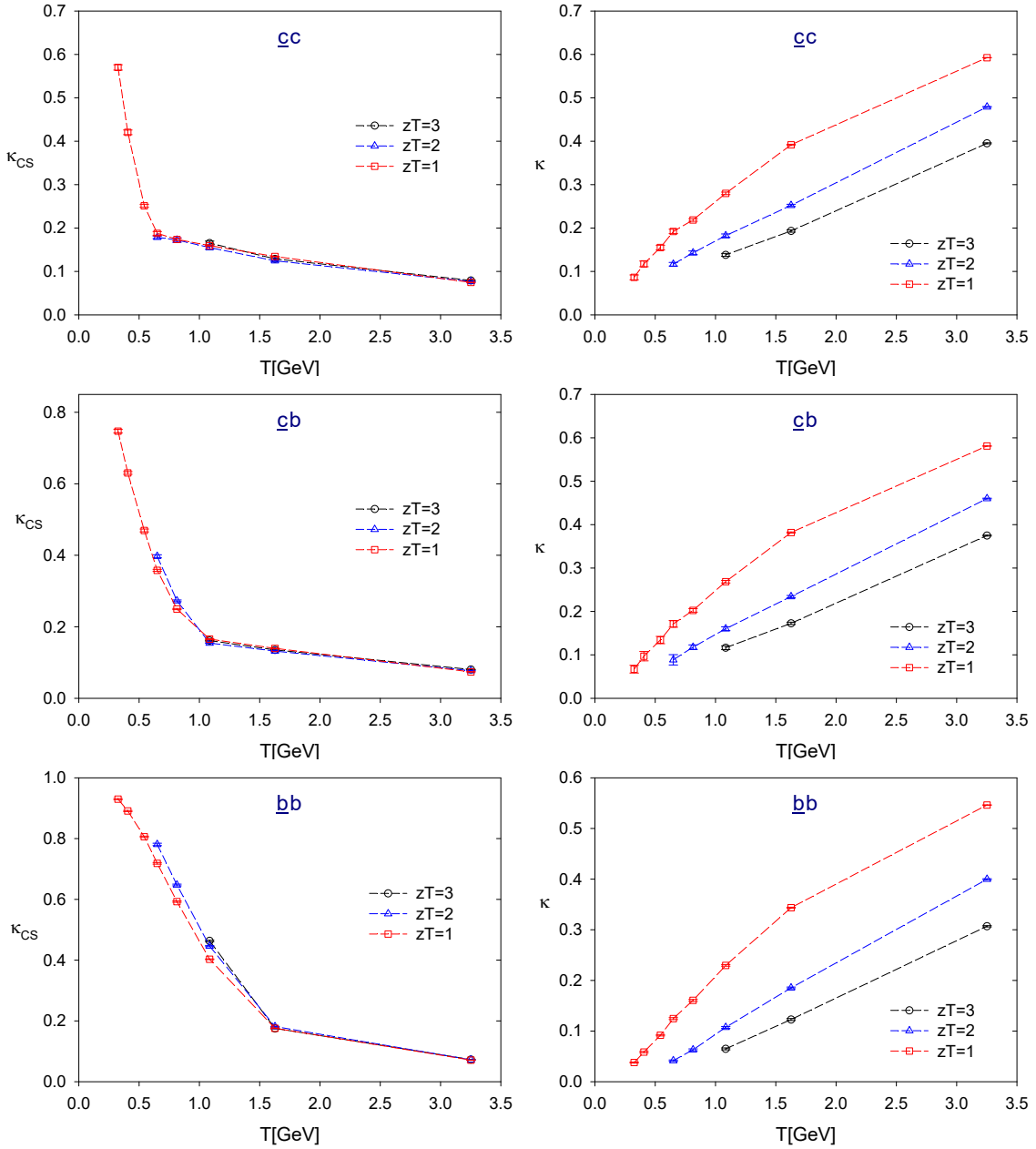


FIG. 6: The chiral-spin symmetry breaking and fading parameters of $(\bar{c}c, \bar{c}b, \bar{b}b)$ mesons.



flavor contents, and for all values of ϵ_{cs} and ϵ_{fcs} sampling from (0.1, 0.15, 0.20). Here we do not extrapolate T smaller than 325 MeV (the lowest temperature of the gauge ensembles). Thus for T windows with lower bounds less than 325 MeV, they are denoted by “<325 MeV” in the Tables V-VI. Similarly, for those which cannot be determined reliably with extrapolation to T less than 650 MeV, they are denoted by “<650 MeV”.

TABLE V: The approximate ranges of T satisfying the criterion (17) at $zT = 2$ for ten flavor contents. The table lists all nonzero windows of T for all values of ϵ_{cs} and ϵ_{fcs} sampling from (0.1, 0.15, 0.20). Each T window is in units of MeV, with uncertainties ~ 10 MeV on both ends of the window.

| ϵ_{cs} | ϵ_{fcs} | $\bar{u}d$ | $\bar{u}s$ | $\bar{s}s$ | $\bar{u}c$ | $\bar{s}c$ | $\bar{u}b$ | $\bar{s}b$ | $\bar{c}c$ | $\bar{c}b$ | $\bar{b}b$ |
|-----------------|------------------|------------|------------|------------|------------|------------|------------|------------|------------|------------|------------|
| 0.20 | 0.20 | 584-1169 | 585-1169 | 584-1169 | 515-1171 | 514-1172 | <325-1239 | <325-1243 | <650-1220 | 979-1376 | 1587-1739 |
| 0.20 | 0.15 | 584-782 | 585-782 | 584-782 | 515-776 | 514-779 | <325-824 | <325-831 | <650-862 | 979-1020 | NULL |
| 0.20 | 0.10 | NULL | NULL | NULL | 515-383 | 514-389 | <325-452 | <325-462 | NULL | NULL | NULL |
| 0.15 | 0.20 | NULL | NULL | NULL | NULL | NULL | <325-1239 | <325-1243 | 1173-1220 | 1191-1376 | NULL |
| 0.15 | 0.15 | NULL | NULL | NULL | NULL | NULL | <325-824 | <325-831 | NULL | NULL | NULL |
| 0.15 | 0.10 | NULL | NULL | NULL | NULL | NULL | <325-452 | <325-462 | NULL | NULL | NULL |

TABLE VI: Same as Table V except for $zT = 3$.

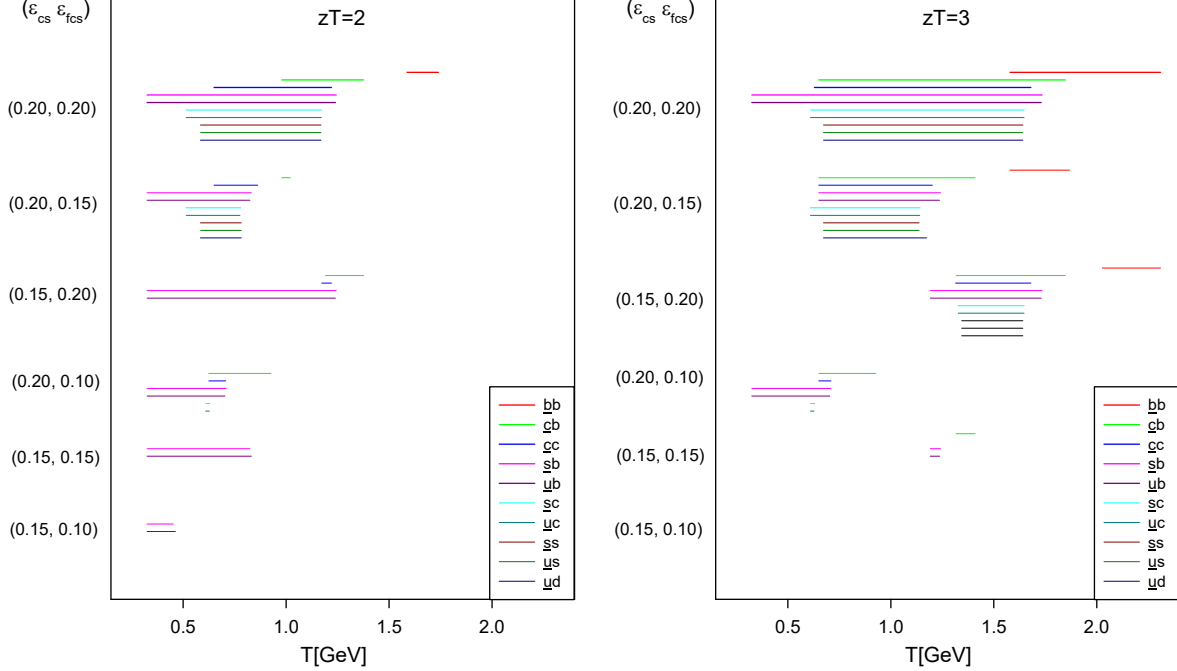
| ϵ_{cs} | ϵ_{fcs} | $\bar{u}d$ | $\bar{u}s$ | $\bar{s}s$ | $\bar{u}c$ | $\bar{s}c$ | $\bar{u}b$ | $\bar{s}b$ | $\bar{c}c$ | $\bar{c}b$ | $\bar{b}b$ |
|-----------------|------------------|------------|------------|------------|------------|------------|------------|------------|------------|------------|------------|
| 0.20 | 0.20 | 673-1641 | 673-1641 | 673-1641 | 610-1647 | 610-1648 | <325-1730 | <325-1734 | <650-1680 | <650-1847 | 1579-2309 |
| 0.20 | 0.15 | 673-1137 | 673-1137 | 673-1137 | 610-1140 | 610-1142 | <325-1236 | <325-1241 | <650-1201 | <650-1409 | 1579-1867 |
| 0.20 | 0.10 | NULL | NULL | NULL | 610-627 | 610-630 | <325-703 | <325-709 | <650-709 | <650-926 | NULL |
| 0.15 | 0.20 | 1344-1641 | 1344-1641 | 1344-1641 | 1327-1647 | 1327-1648 | 1191-1730 | 1191-1734 | 1314-1680 | 1317-1847 | 2027-2309 |
| 0.15 | 0.15 | NULL | NULL | NULL | NULL | NULL | 1191-1236 | 1191-1241 | NULL | 1317-1409 | NULL |

For visualization, we present the nonzero T windows in Fig. 7 for values satisfying $(\epsilon_{cs}, \epsilon_{fcs}) \leq (0.20, 0.20)$. Note that for clarity, the lower bounds of the windows labeled as (< 325 MeV) and (< 650 MeV) in Tables V-VI are plotted to begin at 325 MeV and 650 MeV, respectively.

In lattice QCD simulations with physical (u, d, s, c, b) quarks in a sufficiently large volume, such as on $180^3 \times N_t$ lattices with $a \sim 0.03$ fm, a broader temperature range should be achievable than what is covered in this study. Consequently, the lower bounds of the T windows labeled as (< 325 MeV) and (< 650 MeV) could start at temperatures lower than those shown in Fig. 7.

From Tables V-VI and Fig. 7, we can see that the T windows of the $SU(2)_{CS}$ symmetry are dominated by the channels of vector mesons of $\bar{u}b$ and $\bar{s}b$ (i.e, the b -mesons with heavy-light quarks), since the lower bounds of their T windows begin at the lowest T among all channels

FIG. 7: The windows of T satisfying the criterion (17) for the $SU(2)_{CS}$ symmetry are plotted for ten flavor contents and a range of $(\epsilon_{cs}, \epsilon_{fcs})$, according to the data in Tables V-VI.



and they do not shrink to zero as the precision of $SU(2)_{CS}$ symmetry gets higher with smaller ϵ_{cs} or ϵ_{fcs} down to $(0.15, 0.10)$ at $zT = 2$ and $(0.15, 0.15)$ at $zT = 3$. Besides the channels of vector mesons of $\bar{u}b$ and $\bar{s}b$, the next most prominent channel is $\bar{c}b$. This suggests that the most attractive vector meson channels to detect the emergence of $SU(2)_{CS}$ symmetry are in the $\bar{u}b$ and $\bar{s}b$ sectors, which may have phenomenological implications to the observation of the $SU(2)_{CS}$ symmetry in relativistic heavy ion collision experiments such as those at LHC and RHIC. Moreover, the results of Tables V-VI and Fig. 7 also suggest that the hadronlike objects, in particular, in the channels of $\bar{s}b$ and $\bar{u}b$, are more likely to be predominantly bound by the chromoelectric interactions into color singlets at the temperatures inside their T windows of the $SU(2)_{CS}$ symmetry, since the noninteracting theory with free quarks does not possess the $SU(2)_{CS}$ symmetry at all.

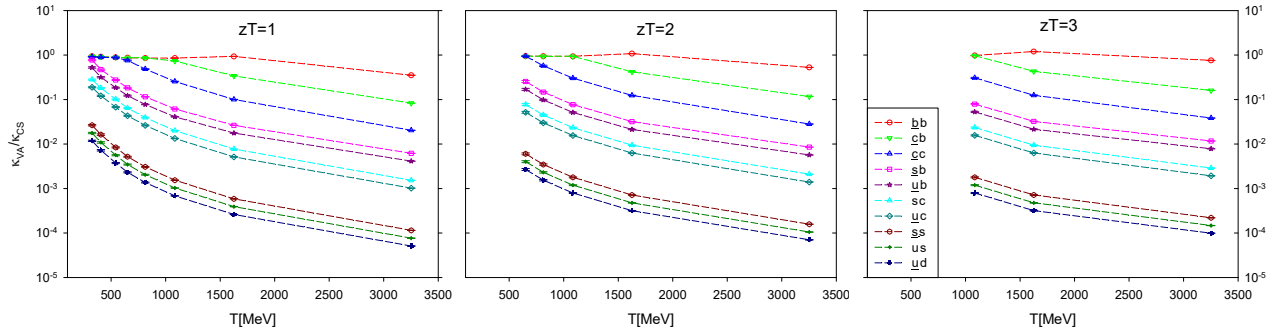
At this point, it is interesting to compare the T windows of the $(\bar{s}s, \bar{s}c, \bar{c}c)$ sectors between the $N_f = 2 + 1 + 1$ QCD at the physical point [5] and this work. For example, for $zT = 2$ and $\epsilon_{cs} = \epsilon_{fcs} = 0.20$, we have the results in Table VII.

TABLE VII: Comparison of the T windows of the emergent $SU(2)_{CS}$ symmetry between $N_f = 2 + 1 + 1$ and $N_f = 2 + 1 + 1 + 1$ lattice QCD.

| flavor content | $N_f = 2 + 1 + 1$ [5] | $N_f = 2 + 1 + 1 + 1$ (this work) |
|----------------|-----------------------|-----------------------------------|
| $\bar{s}s$ | 610-730 MeV | 584-1169 MeV |
| $\bar{s}c$ | 555-740 MeV | 514-1172 MeV |
| $\bar{c}c$ | 555-820 MeV | < 650-1220 MeV |

Obviously, the T windows of the emergent $SU(2)_{CS}$ symmetry in $N_f = 2 + 1 + 1 + 1$ lattice QCD are wider than those in $N_f = 2 + 1 + 1$ lattice QCD, especially for the upper ends of the T windows. At this moment, it is unclear whether this attractive feature is due to the incorporation of the dynamical b quark and/or the smaller lattice spacing (closer to the continuum limit) in this work. If this turns out to be the case, it would imply a higher likelihood of observing the emergent $SU(2)_{CS}$ symmetry in realistic high-temperature QCD settings - specifically, in relativistic heavy-ion collision experiments at facilities like the LHC and RHIC, as well as in future electron-ion collision experiments at planned electron-ion colliders.

FIG. 8: The ratio of the chiral symmetry breaking parameter κ_{VA} and the chiral-spin symmetry breaking parameter κ_{CS} as a function of T , for all flavor combinations and $zT = 1, 2$, and 3 respectively.



Finally, we compare the precision of symmetry between the $SU(2)_{CS}$ chiral-spin symmetry and the $SU(2)_L \times SU(2)_R$ chiral symmetry. To this end, we compute the ratio of their symmetry breaking parameters, κ_{VA}/κ_{CS} for all flavor combination, as shown in Fig. 8, for $zT = 1, 2$, and 3 respectively.

Evidently, for each flavor combination, the ratio κ_{VA}/κ_{CS} is a monotonic decreasing function of T , and it is almost constant for all zT at fixed T . This immediately implies the emergence of $SU(2)_{CS} \times SU(2)_L \times SU(2)_R$ symmetry once the $SU(2)_{CS}$ symmetry emerges in the T windows satisfying the criterion (17). Further, this suggests the possible manifestation of a larger $SU(4)$ symmetry which contains $SU(2)_{CS} \times SU(2)_L \times SU(2)_R$ as a subgroup [7, 8]. To investigate the full $SU(4)$ symmetry, it is necessary to examine the degeneracies of $SU(4)$ multiplets, including flavor singlets of $J = 1$ mesons. The z -correlators for these multiplets involve disconnected diagrams, which are not included in this study. We will address this by analyzing the degeneracies in the chiral susceptibilities of the multiplets, using all-to-all quark propagators estimated with Z_2 noise.

Moreover, the hierarchy of the ratio $R \equiv \kappa_{VA}/\kappa_{CS}$ is exactly the same as (11) and (12), in the order of

$$R^{\bar{u}d} < R^{\bar{u}s} < R^{\bar{s}s} < R^{\bar{u}c} < R^{\bar{s}c} < R^{\bar{u}b} < R^{\bar{s}b} < R^{\bar{c}c} < R^{\bar{c}b} < R^{\bar{b}b}, \quad (18)$$

for all zT at fixed T . However, this does not necessarily imply that the hierarchy of emergence of $SU(2)_{CS}$ symmetry agrees with (18), since the fading of $SU(2)_{CS}$ has to be taken into account. This can be seen clearly from the T windows for the emergence of $SU(2)_{CS}$ in Tables V-VI and Fig. 7.

Now, if we consider κ_{CS} and κ_{VA} on an equal footing, then according to Fig. 8, the $SU(2)_L \times SU(2)_R$ chiral symmetry (as well as $U(1)_A$, since $\kappa_{TX} \simeq \kappa_{VA}$) is significantly more precise than the $SU(2)_{CS}$ chiral-spin symmetry in the $(\bar{u}d, \bar{u}s, \bar{s}s)$ sectors involving light quarks, since $\kappa_{VA}/\kappa_{CS} \lesssim 10^{-2}$. In the heavy-light quark sectors $(\bar{u}c, \bar{s}c, \bar{u}b, \bar{s}b)$, the chiral symmetry remains slightly more precise than the chiral-spin symmetry, with $\kappa_{VA}/\kappa_{CS} \lesssim 0.5$. However, in the sectors $(\bar{c}c, \bar{c}b, \bar{b}b)$ containing only heavy quarks, the chiral and chiral-spin symmetries are of comparable precision, as indicated by $\kappa_{VA}/\kappa_{CS} \lesssim 1$. This gives a qualitative picture how the chiral-spin symmetry versus the chiral symmetry changes with respect to the quark content.

IV. Concluding remarks

In this study, we have generated eight gauge ensembles of $N_f = 2 + 1 + 1 + 1$ lattice QCD with physical (s, c, b) quarks but unphysically heavy u/d quarks, on the $40^3 \times (20, 16, 12, 10, 8, 6, 4, 2)$ lattices with lattice spacing $a \sim 0.030$ fm, for temperatures in the range of 325-3250 MeV, as summarized in Table I.

Using these eight gauge ensembles with $a \sim 0.030$ fm, we computed the meson z -correlators for the complete set of Dirac bilinears (scalar, pseudoscalar, vector, axial vector, tensor vector, and axial-tensor vector), and each for ten combinations of quark flavors ($\bar{u}d$, $\bar{u}s$, $\bar{s}s$, $\bar{u}c$, $\bar{s}c$, $\bar{u}b$, $\bar{s}b$, $\bar{c}c$, $\bar{c}b$, $\bar{b}b$). Then we use the criteria (3) and (6) to determine T_c and T_1 for each flavor combination, and obtain the hierarchy of restoration of chiral symmetry, in the order of

$$T_{c1}^{\bar{u}d} < T_{c1}^{\bar{u}s} < T_{c1}^{\bar{s}s} < T_{c1}^{\bar{u}c} < T_{c1}^{\bar{s}c} < T_{c1}^{\bar{u}b} < T_{c1}^{\bar{s}b} < T_{c1}^{\bar{c}c} < T_{c1}^{\bar{c}b} < T_{c1}^{\bar{b}b}, \quad T_{c1} \equiv \max(T_c, T_1),$$

which immediately gives the hierarchical restoration of chiral symmetry in $N_f = 2 + 1 + 1 + 1$ QCD, i.e., from the manifestation of $SU(2)_L \times SU(2)_R \times U(1)_A$ chiral symmetry of (u, d) quarks at $T_{c1}^{\bar{u}d}$ to the $SU(3)_L \times SU(3)_R \times U(1)_A$ chiral symmetry of (u, d, s) quarks at $T_{c1}^{\bar{s}s}$, then to the $SU(4)_L \times SU(4)_R \times U(1)_A$ chiral symmetry of (u, d, s, c) quarks at $T_{c1}^{\bar{c}c}$, and finally to the $SU(5)_L \times SU(5)_R \times U(1)_A$ chiral symmetry of (u, d, s, c, b) quarks at $T_{c1}^{\bar{b}b}$.

One of the key phenomenological outcomes of the hierarchical restoration of chiral symmetry is the sequential pattern of hadron dissolution as the temperature is increased successively, resulting in a hierarchy in both the dissolution of hadrons and their suppression within the quark-gluon plasma. Theoretically, a meson with quark content $\bar{q}Q$ dissolves entirely when \bar{q} and Q become deconfined. This occurs when the screening mass of the meson exceeds that of a corresponding noninteracting theory with free quarks of the same masses of q and Q . It is expected that $m_{\text{scr}}^{\bar{q}Q} \geq m_{\text{scr}}^{\bar{q}Q(\text{free})}$ at a temperature $T_d^{\bar{q}Q} \gtrsim T_{c1}^{\bar{q}Q}$, where the chiral symmetry $SU(2)_L \times SU(2)_R \times U(1)_A$ of $\bar{q}\Gamma Q$ has been effectively restored. For $N_f = 2 + 1 + 1 + 1$ lattice QCD, this implies that the hierarchy of meson dissolution is exactly the same as that of chiral symmetry restoration (13), specifically:

$$T_d^{\bar{u}d} < T_d^{\bar{u}s} < T_d^{\bar{s}s} < T_d^{\bar{u}c} < T_d^{\bar{s}c} < T_d^{\bar{u}b} < T_d^{\bar{s}b} < T_d^{\bar{c}c} < T_d^{\bar{c}b} < T_d^{\bar{b}b}.$$

This hierarchy predicts the gradual suppression of mesons within the quark-gluon plasma, potentially observable in relativistic heavy-ion collision experiments, such as those conducted at the LHC and RHIC. This notion builds on the pioneering work [13], which proposed that the dissolution of J/ψ mesons in the quark-gluon plasma would manifest as suppressed production in heavy-ion collision experiments.

Regarding the emergent $SU(2)_{CS}$ chiral-spin symmetry, it is intriguing to observe that the temperature windows meeting the criterion (17) are dominated by the channels of heavy vector mesons with flavor contents $(\bar{u}b, \bar{s}b)$, as indicated by Tables V-VI and Fig. 7. These results represent the first findings in lattice QCD and suggest that, within their respective temperature windows, hadronlike states—especially $\bar{u}b$ and $\bar{s}b$ vector mesons—are likely bound into color singlets by chromoelectric interactions. This is notable because the noninteracting theory with free quarks lacks any $SU(2)_{CS}$ symmetry. Furthermore, these findings offer valuable insights for exploring the emergent $SU(2)_{CS}$ symmetry in relativistic heavy-ion collision experiments, such as those conducted at the LHC and RHIC, by focusing on vector meson channels with $\bar{u}b$ and $\bar{s}b$ quark contents.

Furthermore, based on the comparison between $N_f = 2 + 1 + 1$ and $N_f = 2 + 1 + 1 + 1$ lattice QCD results in Table VII, we propose that the T windows for the emergence of $SU(2)_{CS}$ symmetry in physical QCD—obtained via lattice QCD with physical (u, d, s, c, b) quarks and extrapolated to the continuum limit—are likely to be broader than those observed in unphysical lattice QCD that lack one or more of the following conditions: dynamical c or b quarks, physical quark masses, or extrapolation to the continuum limit.

To understand the nature of mesonlike states in the $J = 1$ channels (i.e., $V_k, A_k, T_k,$ and X_k) which are relevant to the emergent $SU(2)_{CS}$ symmetry, it is essential to analyze the behavior of their spectral functions as the temperature increases. If bound-state peaks are found within the temperature ranges where the $SU(2)_{CS}$ symmetry holds, and these peaks gradually broaden and eventually vanish as T rises beyond these ranges, it would suggest that the degrees of freedom in these mesonlike objects correspond to color-singlet (melting) mesons, as opposed to deconfined quarks and gluons. To investigate this, one could consider extending the method used in Refs. [14–16] for $J = 0$ mesons to the $J = 1$ mesons. Additionally, it is necessary to compute the spatial z -correlators of vector mesons to high

precisions, free of the contribution of unphysical meson states even at large distances, in order to reliably extract the damping factor for each $J = 1$ meson channel. The prescription used in Ref. [4] (to compute two sets of quark propagators with periodic and antiperiodic boundary conditions in the z direction) provides an effective way to eliminate the contribution of unphysical meson states to the z -correlators and offers a promising way to achieve this goal.

ACKNOWLEDGEMENTS

The author is grateful to Academia Sinica Grid Computing Center and National Center for High Performance Computing for the computer time and facilities. This work is supported by the National Science and Technology Council (Grants No. 108-2112-M-003-005, No. 109-2112-M-003-006, No. 110-2112-M-003-009), and Academia Sinica Grid Computing Centre (Grant No. AS-CFII-112-103).

-
- [1] C. E. DeTar and J. B. Kogut, “The Hadronic Spectrum of the Quark Plasma,” [Phys. Rev. Lett.](#) **59**, 399 (1987).
 - [2] C. E. Detar and J. B. Kogut, “Measuring the Hadronic Spectrum of the Quark Plasma,” [Phys. Rev. D](#) **36**, 2828 (1987).
 - [3] A. Bazavov, S. Dentinger, H. T. Ding, P. Hegde, O. Kaczmarek, F. Karsch, E. Laermann, A. Lahiri, S. Mukherjee and H. Ohno, *et al.* “Meson screening masses in (2+1)-flavor QCD,” [Phys. Rev. D](#) **100**, no.9, 094510 (2019) [arXiv:1908.09552 [hep-lat]].
 - [4] T. W. Chiu, “Symmetries of meson correlators in high-temperature QCD with physical (u/d,s,c) domain-wall quarks,” [Phys. Rev. D](#) **107**, no.11, 114501 (2023) [arXiv:2302.06073 [hep-lat]].
 - [5] T. W. Chiu, “Symmetries of spatial correlators of light and heavy mesons in high temperature lattice QCD,” [Phys. Rev. D](#) **110**, no.1, 014502 (2024) [arXiv:2404.15932 [hep-lat]].
 - [6] T. W. Chiu, “Beauty mesons in $N_f=2+1+1+1$ lattice QCD with exact chiral symmetry,” [Phys. Rev. D](#) **102**, no.3, 034510 (2020) [arXiv:2004.02142 [hep-lat]].
 - [7] L. Y. Glozman, “SU(4) symmetry of the dynamical QCD string and genesis of hadron spectra,” [Eur. Phys. J. A](#) **51**, no.3, 27 (2015) [arXiv:1407.2798 [hep-ph]].

- [8] L. Y. Glozman and M. Pak, “Exploring a new SU(4) symmetry of meson interpolators,” *Phys. Rev. D* **92**, no.1, 016001 (2015) [arXiv:1504.02323 [hep-lat]].
- [9] C. Rohrhofer, Y. Aoki, G. Cossu, H. Fukaya, C. Gattringer, L. Y. Glozman, S. Hashimoto, C. B. Lang and S. Prelovsek, “Symmetries of spatial meson correlators in high temperature QCD,” *Phys. Rev. D* **100**, no.1, 014502 (2019) [arXiv:1902.03191 [hep-lat]].
- [10] N. J. Evans, S. D. H. Hsu and M. Schwetz, “Topological charge and U(1)-A symmetry in the high temperature phase of QCD,” *Phys. Lett. B* **375**, 262-266 (1996) [arXiv:hep-ph/9601361 [hep-ph]].
- [11] M. C. Birse, T. D. Cohen and J. A. McGovern, “U(1)-A symmetry and correlation functions in the high temperature phase of QCD,” *Phys. Lett. B* **388**, 137-140 (1996) [arXiv:hep-ph/9608255 [hep-ph]].
- [12] T. D. Cohen and X. D. Ji, “Chiral multiplets of hadron currents,” *Phys. Rev. D* **55**, 6870-6876 (1997) [arXiv:hep-ph/9612302 [hep-ph]].
- [13] T. Matsui and H. Satz, “ J/ψ Suppression by Quark-Gluon Plasma Formation,” *Phys. Lett. B* **178**, 416-422 (1986)
- [14] J. Bros and D. Buchholz, “Particles and propagators in relativistic thermo field theory,” *Z. Phys. C* **55**, 509-514 (1992)
- [15] J. Bros and D. Buchholz, “Asymptotic dynamics of thermal quantum fields,” *Nucl. Phys. B* **627**, 289-310 (2002) [arXiv:hep-ph/0109136 [hep-ph]].
- [16] P. Lowdon and O. Philipsen, “Pion spectral properties above the chiral crossover of QCD,” *JHEP* **10**, 161 (2022) [arXiv:2207.14718 [hep-lat]].